SIAM J. SCI. COMPUT.
Vol. 44, No. 1, pp. B100–B121

A SPECTRALLY ACCURATE NUMERICAL METHOD FOR COMPUTING THE BOGOLIUBOV–DE GENNES EXCITATIONS OF DIPOLAR BOSE–EINSTEIN CONDENSATES*

QINGLIN TANG†, MANTING XIE‡, YONG ZHANG§, AND YUQING ZHANG‡

Abstract. In this paper, we propose an efficient and robust numerical method to study the elementary excitation of dipolar Bose–Einstein condensates, which is governed by the Bogoliubov–de Gennes equations (BdGEs) with nonlocal dipole-dipole interaction, around the mean field ground state. Analytical properties of the BdGEs are investigated, which could serve as benchmarks for the numerical methods. To evaluate the nonlocal interactions accurately and efficiently, we propose a new simple Fourier spectral convolution (SFSC) method. Then, integrating SFSC with the standard Fourier spectral method for spatial discretization and implicitly restarted Arnoldi methods (IRAM) for the eigenvalue problem, we derive an efficient and spectrally accurate method, named the SFSC-IRAM, for the BdGEs. Ample numerical tests are provided to illustrate the accuracy and efficiency. Finally, we apply the new method to study systematically the excitation spectrum and Bogoliubov amplitudes around the ground state with different parameters in different spatial dimensions.

Key words. Bogoliubov–de Gennes excitations, dipolar Bose–Einstein condensates, convolution-type nonlocal interaction, Fourier spectral convolution method

AMS subject classifications. 65M70, 68Q25, 65T50, 65R20

DOI. 10.1137/21M1401048

1. Introduction.

Since the realization of Bose–Einstein condensates (BECs) of dipolar quantum gases [2, 27, 37], we have witnessed unique and novel phenomena, such as the roton-maxon spectrum[35, 40], the self-bound droplet state [23, 44], and the newfangled vortex lattice patterns [38], due to the fundamental anisotropic and long-range magnetic/electric dipole-dipole interatomic interaction. To understand the stability of stationary states of a BEC, it is important to study its elementary excitations around the stationary states [35, 40]. The first experimental measurements of the lowest collective modes of BECs were carried out in [32]. Great efforts have been made to experimentally, theoretically, and numerically study the collective excitations of BECs since then [20, 24, 28, 29, 33, 39, 40, 43, 49].

At a temperature much lower than the critical value T_c, the properties of the BEC with long-range dipole-dipole interaction (DDI) are well characterized by the macroscopic complex-valued wave function $\psi(\boldsymbol{x}, t)$ whose evolution could be well governed by the three-dimensional (3D) Gross–Pitaevskii equation (GPE) with DDI term [5, 9, 10, 26, 52]. Moreover, the 3D GPE with some special highly anisotropic external

*Submitted to the journal's Computational Methods in Science and Engineering section February 24, 2021; accepted for publication (in revised form) August 23, 2021; published electronically January 18, 2022.

https://doi.org/10.1137/21M1401048

Funding: The work of the first author was supported by the National Natural Science Foundation of China (11971335) and by the Institutional Research Fund from Sichuan University (2020SCUNL110). The work of the second author was supported by the National Science Foundation of China (12001402 and 12071343).

†School of Mathematics, State Key Laboratory of Hydraulics and Mountain River Engineering, Sichuan University, Chengdu 610064, China (qinglin_tang@scu.edu.cn).

‡Center for Applied Mathematics, Tianjin University, Tianjin 300072, China (mtxie@tju.edu.cn, 17831108357@163.com).

§Corresponding author. Center for Applied Mathematics, Tianjin University, Tianjin 300072, China (Zhang_Yong@tju.edu.cn).

potential could be reduced to an effective two-dimensional (2D) equation [15, 17, 10]. In dimensionless form, the d-dimensional ($d = 2$ or 3) GPE with DDI term could be unified as [9, 17, 15]

$$i\partial_t \psi(\boldsymbol{x}, t) = \left[-\frac{1}{2}\nabla^2 + V(\boldsymbol{x}) + \beta|\psi|^2 + \lambda\,\Phi\right]\psi, \quad \boldsymbol{x} \in \mathbb{R}^d, \quad t > 0, \tag{1}$$

$$\Phi(\boldsymbol{x}, t) := (U * |\psi|^2)(\boldsymbol{x}, t), \tag{2}$$

$$\psi(\boldsymbol{x}, 0) = \psi_0(\boldsymbol{x}), \tag{3}$$

where t denotes time, $\boldsymbol{x} = (x, y)^T \in \mathbb{R}^2$ and/or $\boldsymbol{x} = (x, y, z)^T \in \mathbb{R}^3$ is the Cartesian coordinate vector, and $*$ represents the convolution operator with respect to the spatial variable. $V(\boldsymbol{x})$ is a real-valued external potential which is case dependent, and one common choice is the harmonic trapping potential which reads as

$$V(\boldsymbol{x}) = \frac{1}{2}\begin{cases} \gamma_x^2 x^2 + \gamma_y^2 y^2, & d = 2, \\ \gamma_x^2 x^2 + \gamma_y^2 y^2 + \gamma_z^2 z^2, & d = 3. \end{cases} \tag{4}$$

Here, $\gamma_\alpha > 0$ ($\alpha = x, y, z$) are dimensionless constants proportional to the trapping frequency in ν-direction. Moreover, the dimensionless constant β and λ characterize, respectively, the short-range contact interaction and long-range DDI. The interaction kernel $U(\boldsymbol{x})$ reads as

$$U(\boldsymbol{x}) = \begin{cases} -\delta(\boldsymbol{x}) - 3\,\partial_{\boldsymbol{nn}}\left(\frac{1}{4\pi|\boldsymbol{x}|}\right), & \boldsymbol{x} \in \mathbb{R}^3, \\ -\frac{3}{2}\left(\partial_{\boldsymbol{n}_\perp \boldsymbol{n}_\perp} - n_3^2\nabla_\perp^2\right)\left(\frac{1}{2\pi|\boldsymbol{x}|}\right), & \boldsymbol{x} \in \mathbb{R}^2. \end{cases} \tag{5}$$

Here, $\boldsymbol{n} = (n_1, n_2, n_3)^T \in \mathbb{R}^3$ is a given unit vector representing the dipole moment, $\partial_{\boldsymbol{n}} = \boldsymbol{n} \cdot \nabla, \partial_{\boldsymbol{nn}} = \partial_{\boldsymbol{n}}(\partial_{\boldsymbol{n}})$, $\nabla_\perp = (\partial_x, \partial_y)^T$, $\boldsymbol{n}_\perp = (n_1, n_2)^T$, and $\partial_{\boldsymbol{n}_\perp} = \boldsymbol{n}_\perp \cdot \nabla_\perp, \partial_{\boldsymbol{n}_\perp \boldsymbol{n}_\perp} = \partial_{\boldsymbol{n}_\perp}(\partial_{\boldsymbol{n}_\perp})$.

The time-dependent GPE (1)–(3) conserves two important quantities: the mass of the wave function

$$N(\psi(\cdot, t)) := \|\psi(\boldsymbol{x}, t)\|^2 = \int_{\mathbb{R}^d} |\psi|^2 \mathrm{d}\boldsymbol{x} \equiv N(\psi(\cdot, 0)), \qquad t \geq 0, \tag{6}$$

and the energy *per particle*

$$E(\psi(\cdot, t)) = \int_{\mathbb{R}^d} \left[\frac{1}{2}|\nabla\psi|^2 + V(\boldsymbol{x})|\psi|^2 + \frac{\beta}{2}|\psi|^4 + \frac{\lambda}{2}\Phi|\psi|^2\right] \mathrm{d}\boldsymbol{x} \equiv E(\psi(\cdot, 0)), \quad t \geq 0. \tag{7}$$

Plug the ansatz $\psi(\boldsymbol{x}, t) = e^{i\mu_s t}\phi_s(\boldsymbol{x})$ into (1); one obtains the time-independent GPE for the stationary state $\phi_s(\boldsymbol{x})$

$$\mu_s \phi_s(\boldsymbol{x}) = \left[-\frac{1}{2}\nabla^2 + V(\boldsymbol{x}) + \beta|\phi_s|^2 + \lambda\,(U * |\phi_s|^2)\right]\phi_s(\boldsymbol{x}), \quad \|\phi_s(\boldsymbol{x})\| = 1, \tag{8}$$

which is also a nonlinear eigenvalue problem. The corresponding eigenvalue $\mu_s \in \mathbb{R}$ is also called chemical potential which could be evaluated from $\phi_s(\boldsymbol{x})$ as follows:

$$\mu_s = \int_{\mathbb{R}^d} \left[\frac{1}{2}|\nabla\phi_s|^2 + V(\boldsymbol{x})|\phi_s|^2 + \beta|\phi_s|^4 + \lambda\,(U * |\phi_s|^2)\,|\phi_s|^2\right] \mathrm{d}\boldsymbol{x}. \tag{9}$$

The ground state $\phi_g(\boldsymbol{x})$, which is the stationary state of the lowest energy, could also be interpreted as the global minimizer of the following nonconvex minimization problem:

$$\phi_g(\boldsymbol{x}) = \arg\min_{\phi\in\mathcal{S}} \mathcal{E}(\phi), \tag{10}$$

with $\mathcal{S} := \{\phi(\boldsymbol{x}) \mid \|\phi\|^2 := \int_{\mathbb{R}^d} |\phi(\boldsymbol{x})|^2 \mathrm{d}\boldsymbol{x} = 1,\ E(\phi) < \infty\}$. The GPE (1)–(3) proves to be valid for the dipolar BEC on the mean field level [16, 35, 52]; however, it fails to describe the quantum fluctuation [28] of the condensate. Hence, one needs to go beyond the mean field theory, and the very first step is to investigate the collective excitation so as to capture the many body effect of interatomic interactions. The collective excitation could be analyzed via elementary excitation of the system governed by GPE (1). Under proper assumption of the dipolar BEC, the elementary excitation around the mean field stationary state could be well described within the Bogoliubov theory, which resulted in the celebrated Bogoliubov–de Gennes equations (BdGEs) [8, 29, 24, 36, 40]. To date, the analysis works on the elementary excitations in BECs are mainly composed of the GPE for describing the condensed part and the Bogoliubov theory for describing the noncondensed part, respectively [28].

Great enthusiasm has been stimulated to investigate BdGEs in physics literature [28, 43] in the past few decades, most of which are about nondipolar systems. Based on the low energy excitation of a dilute Boson gas in harmonic traps, Stringari [43] obtains the long wave excitation frequency of a trapped BEC in a Thomas–Fermi regime. A method to find analytical solutions of BdGEs for the low-lying collective excitation in harmonic trap potential beyond the Thomas–Fermi regime was proposed by Hu, Huang, and Ma [28]. Along the numerical front, there have been quite a few developments. Edwards et al. and Morgan et al. [20, 39] applied the finite difference method and solved the sparse algebraic eigenvalue system using the ARPACK library. Danaila et al. investigated the BdGEs of a multicomponent BEC with the finite element method [19]. Gao and Cai systematically studied BdGEs for the classical GPE and proposed several efficient algorithms, including the compact finite difference method and sine spectral method [24]. In contrast, there are few theoretical studies on the excitation of dipolar BECs. For the numerical studies, there are some papers that mainly consider the lower-dimensional cases ($d = 1$ or 2). For example, Jia, Wang, and Yi [29] studied the low-lying collective excitation of the rotating quasi-2D system with the Fourier spectral method, and Ronen, Bortolotti, and Bohn and Wilson, Ronen, and Bohn [40, 49] developed an algorithm based on the one-dimensional discrete Hankel transform for a cylindrically symmetric system. Those works are either mainly for lower-dimensional cases or systems with a specific symmetric structure, and they are disadvantageous in evaluating the nonlocal DDI.

Furthermore, to the best of our knowledge, there were no systematical studies on BdGEs in the context of dipolar BEC from the mathematical standpoint. Hence, it is necessary to develop mathematical theories and to construct accurate and efficient numerical methods to solve the corresponding BdGEs. To numerically investigate the elementary excitations, the main challenge lies in (i) a robust solver for the eigenvalue problem, i.e., BdGEs; (ii) an accurate and efficient stationary state (8) and/or a ground states solver; (iii) an accurate DDI fast solver that would play a decisive role in the whole numerical method, particularly in high spatial dimensions. Fortunately, the computation of nonlocal DDI has been studied quite extensively, and many effective algorithms have been proposed, such as the sine spectral method [12, 9, 10], the

nonuniform fast Fourier transform method [13, 14, 31], the Gaussian-sum method [21], the kernel truncation method [40, 41, 47], and the anisotropic truncated kernel method (ATKM) [25]. The smooth and fast-decaying density $\rho := |\psi|^2$ can be well approximated by the Fourier spectral method, and it is reasonable to expect spectral accuracy with the same efficiency when computing the nonlocal interactions. In fact, all of the last three methods can achieve spectral accuracy within $O(N \log N)$ operations, where N is the number of unknowns. However, the prefactors in front of $O(N \log N)$ are usually very large; hence improvement is required to achieve better efficiency, especially for problems in high space dimension. In this paper, starting from the density's Fourier spectral approximation, we will propose an even simpler method (in section 3.2) to compute the nonlocal DDI. The proposed nonlocal solver achieves spectral accuracy with an even better complexity, i.e., a smaller prefactor in $O(N \log N)$.

As for the computation of stationary/ground states, various numerical methods have been proposed for the (non)dipolar BEC [3, 4, 9, 10, 11, 13, 18, 30, 47, 48, 50, 51], among which the preconditioned conjugate gradient (PCG) method [4] was evidenced to be one of the most efficient solvers. Recently, Tang et al. [45] incorporated the ATKM for the DDI evaluation into the PCG method to compute the stationary state of a dipolar BEC. The resulted PCG-ATKM is spectrally accurate, simple to implement, and fast (with a $O(N \log N)$ complexity). We will apply the PCG-ATKM to precompute the stationary/ground state ϕ_s for the BdGEs. With the Fourier spectral discretization in space, the resulted discrete eigensystem, i.e., the discrete BdGEs, is densely populated, which shall render prohibitively huge memory costs with explicit matrix storage. Therefore, it is necessary to provide an efficient matrix-free operator-function evaluation during the iterative eigenvalue process. In this paper, we will apply the matrix-free implicitly restarted Arnoldi methods (IRAM), implemented efficiently via ARPACK with reverse communication interface, to solve the resulted discrete eigenvalue/vector system. Overall, the main objectives of this paper are threefold:

1. investigate theoretically the mathematical properties of the BdGEs, focusing on their special analytical solution pairs in different regimes;
2. develop an efficient and accurate algorithm, i.e., SFSC, for nonlocal interactions and integrate it with the matrix-free IRAM to solve the discrete BdGEs via ARPACK or its variant;
3. apply the proposed SFSC-IRAM to investigate the excitation spectrum and Bogoliubov amplitudes of the dipolar BEC around ground state with different parameters in two and three dimensions.

The rest of the paper is organized as follows: In section 2, we introduce the BdGEs and derive some analytical properties. In section 3, we present the details of the Fourier spectral method for space discretization and propose the simple Fourier spectral convolution method for computing the nonlocal interactions as well as the approach to compute the discrete BdGEs. Extensive numerical examples are shown in section 4 to confirm the performance of our method, together with some applications to study the solutions to the BdGEs with different parameters in two and three dimensions. Finally, conclusions are drawn in section 5.

2. The BdGEs and its properties.

2.1. The BdGEs. To characterize the elementary excitations of a dipolar BEC, the Bogoliubov theory [8, 24, 36, 40] begins with the stationary state $\phi_s(\boldsymbol{x})$ of the

GPE (1), which is also the solution of the nonlinear eigenvalue problem (8) with chemical potential μ_s (9), and assumes the evolution of GPE (1) is around $\phi_s(\boldsymbol{x})$. The corresponding wave function ψ would then take the form [24, 40]

$$\psi(\boldsymbol{x},t) = e^{-i\mu_s t}\left[\phi_s(\boldsymbol{x}) + p\sum_{j=1}^{\infty}\left(u_j(\boldsymbol{x})e^{-i\omega_j t} + \bar{v}_j(\boldsymbol{x})e^{i\omega_j t}\right)\right],\ \boldsymbol{x}\in\mathbb{R}^d, t>0. \tag{11}$$

Here, $\bar{v}_j$ denotes the complex conjugate of v_j, $0 < p \ll 1$ is a small quantity used to control the population of quasi-particle excitation, $\omega_j \in \mathbb{C}$ is the frequency of the excitations to be determined, and $u_j(\boldsymbol{x})$ and $v_j(\boldsymbol{x})$ are the corresponding Bogoliubov excitation modes satisfying the following normalization condition:

$$\int_{\mathbb{R}^d}\left(|u_j(\boldsymbol{x})|^2 - |v_j(\boldsymbol{x})|^2\right)\mathrm{d}\boldsymbol{x} = 1, \quad j\in\mathbb{Z}^+. \tag{12}$$

Plugging (11) into (1) and (2), collecting the linear terms in p, and separating the frequencies $e^{-i\omega_j t}$ and $e^{i\omega_j t}$, we obtain the following BdGEs:

$$\mathcal{L}_{\mathrm{GP}}u_j + \beta|\phi_s|^2u_j + \beta\phi_s^2\, v_j + \lambda U * \left(\bar{\phi}_s u_j + \phi_s v_j\right)\phi_s = \quad \omega_j\, u_j, \tag{13}$$

$$\mathcal{L}_{\mathrm{GP}}v_j + \beta\bar{\phi}_s^2u_j + \beta|\phi_s|^2v_j + \lambda U * \left(\bar{\phi}_s u_j + \phi_s v_j\right)\bar{\phi}_s = -\omega_j v_j, \tag{14}$$

with

$$\mathcal{L}_{\mathrm{GP}} := -\frac{1}{2}\nabla^2 + V(\boldsymbol{x}) + \beta|\phi_s|^2 + \lambda\Phi_s - \mu_s, \quad \Phi_s = U * |\phi_s|^2. \tag{15}$$

Under the proper assumption, it has been shown that the stationary state $\phi_s(\boldsymbol{x})$ is unique up to a constant phase factor [9] and can be chosen as a real-valued function $\phi_s^R(\boldsymbol{x})$, i.e., $\phi_s(\boldsymbol{x}) = \phi_s^R(\boldsymbol{x})\, e^{i\theta}$ with $\theta\in\mathbb{R}$. It is easy to check that the different choice of ϕ_s with the different phase factor θ only resulted in different Bogoliubov amplitude functions with a phase factor; i.e., if (ω_j, u_j, v_j) solves BdGEs (13) and (14) with ϕ_s, then $(\omega_j, e^{i\theta}\, u_j, e^{-i\theta}\, v_j)$ solves BdGEs (13) and (14) with $e^{i\theta}\phi_s$. Thus, it suffices to consider the real-valued stationary states case, and we shall assume $\phi(\boldsymbol{x})\in\mathbb{R}$ throughout this paper. To simplify the presentation, hereafter we remove all subscripts for u_j, v_j, and w_j and write them indiscriminately as u, v, and w, respectively. Denote operators

$$\begin{aligned} \mathcal{L}_{11} &= \mathcal{L}_{\mathrm{GP}} + \beta\,|\phi_s|^2 + \lambda\,\widehat{\chi}_1, \qquad \mathcal{L}_{12} = \beta\,\phi_s^2 + \lambda\,\widehat{\chi}_2, \\ \mathcal{L}_{22} &= -\mathcal{L}_{\mathrm{GP}} - \beta\,|\phi_s|^2 - \lambda\,\widehat{\chi}_1^*, \qquad \mathcal{L}_{21} = -\beta\bar{\phi}_s^2 - \lambda\,\widehat{\chi}_2^*, \end{aligned} \tag{16}$$

with nonlocal actions $\widehat{\chi}_j$ and $\widehat{\chi}_j^*$ $(j=1,2)$ defined as

$$\begin{aligned} \widehat{\chi}_1(\xi) &:= \phi_s\left[U * (\bar{\phi}_s\xi)\right], \qquad \widehat{\chi}_2(\xi) := \phi_s\left[U * (\phi_s\xi)\right], \\ \widehat{\chi}_1^*(\xi) &:= \bar{\phi}_s\left[U * (\phi_s\xi)\right], \qquad \widehat{\chi}_2^*(\xi) := \bar{\phi}_s\left[U * (\bar{\phi}_s\xi)\right]; \end{aligned} \tag{17}$$

the BdGEs (13) and (14) with constraint (12) could be equivalently recasted as

$$\begin{pmatrix} \mathcal{L}_{11} & \mathcal{L}_{12} \\ \mathcal{L}_{21} & \mathcal{L}_{22} \end{pmatrix}\begin{pmatrix} u \\ v \end{pmatrix} = \omega\begin{pmatrix} u \\ v \end{pmatrix}, \tag{18}$$

with constraint

$$\int_{\mathbb{R}^d}\left(|u(\boldsymbol{x})|^2 - |v(\boldsymbol{x})|^2\right)d\boldsymbol{x} = 1. \tag{19}$$

Specially, for the real-valued stationary state ϕ_s, all the nonlocal operators are identical, i.e., $\widehat{\chi}_1 \equiv \widehat{\chi}_2 \equiv \widehat{\chi}_1^* \equiv \widehat{\chi}_2^*$. By applying a change of variables

$$u(\boldsymbol{x}) = f(\boldsymbol{x}) + g(\boldsymbol{x}), \qquad v(\boldsymbol{x}) = f(\boldsymbol{x}) - g(\boldsymbol{x}), \tag{20}$$

the BdGEs (18) could be simplified as

$$H_+ f(\boldsymbol{x}) = \omega g(\boldsymbol{x}), \qquad H_- g(\boldsymbol{x}) = \omega f(\boldsymbol{x}), \quad \Re\left(\int_{\mathbb{R}^d} (f(\boldsymbol{x})\,\bar{g}(\boldsymbol{x}))\,d\boldsymbol{x}\right) = \frac{1}{4}, \tag{21}$$

which immediately leads to a decoupled linear eigensystem

$$H_- H_+ f(\boldsymbol{x}) = \omega^2 f(\boldsymbol{x}), \qquad H_+ H_- g(\boldsymbol{x}) = \omega^2 g(\boldsymbol{x}). \tag{22}$$

Here, $\Re(\alpha)$ denotes the real part of α, $H_+ := \mathcal{L}_{\rm GP} + 2\beta|\phi_s|^2 + 2\lambda\hat{\chi}_1$, *and* $H_- := \mathcal{L}_{\rm GP}$. One could solve the above decoupled unconstrained eigenvalue problems (22) instead of the coupled constrained system (18), which is common in the physics community [40]. Alternatively, we can directly treat (18) as a linear response problem and solve it by the locally optimal block preconditioned four-dimensional conjugate gradient algorithm or its variants [6, 7].

Due to the nonlocal character of DDI, the BdGEs are very difficult for both analytical and numerical analysis. Only for several low energy excitation modes is it possible to obtain some analytic results by using a Gaussian variational ansatz [35] or the Thomas–Fermi approximation [28]. Here we investigate the typical harmonic trapping potential case (4) and derive some analytical properties of BdGEs, which could serve as benchmarks for testing numerical methods.

2.2. Analytical properties of BdGEs. For general potential $V(\boldsymbol{x})$, we have the following results.

LEMMA 1. *If* $\{u, v, \omega\}$ *(*$\omega \in \mathbb{C}$*) is a solution pair to the BdGEs* (18)*, then* $\{\bar{v}, \bar{u}, -\bar{\omega}\}$ *is also a solution to the BdGEs* (18) *and*

$$(\omega - \bar{\omega}) \int_{\mathbb{R}^d} (|u(\boldsymbol{x})|^2 - |v(\boldsymbol{x})|^2)\,d\boldsymbol{x} = 0. \tag{23}$$

Furthermore, if $u(\boldsymbol{x})$, $v(\boldsymbol{x})$ *satisfy the normalization constraint* (19)*, i.e., the elementary excitations, then the eigenfrequency* ω *is real.*

Proof. Take conjugate of (13) and (14) on both sides; we have

$$\begin{aligned} &\mathcal{L}_{\rm GP}\bar{u} + \beta(\bar{\phi}_s)^2\bar{v} + \beta|\phi_s|^2\bar{u} + \lambda\, U * (\bar{\phi}_s\bar{v} + \phi_s\bar{u})\bar{\phi}_s = \ \bar{\omega}\bar{u}, \\ &\mathcal{L}_{\rm GP}\bar{v} + \beta|\phi_s|^2\bar{v} \ + \beta\phi_s^2\bar{u} \ \ + \ \lambda\, U * (\bar{\phi}_s\bar{v} + \phi_s\bar{u})\phi_s = -\bar{\omega}\bar{v}, \end{aligned}$$

which immediately implies that $\{\bar{v}, \bar{u}, -\bar{\omega}\}$ is also a solution. Multiplying (13) and (14), respectively, by $\bar{u}$ and $\bar{v}$, integrating over $\mathbb{R}^d$, and combining the resulting equations, we obtain

$$\begin{aligned} &\omega \int_{\mathbb{R}^d} (|u(\boldsymbol{x})|^2 - |v(\boldsymbol{x})|^2) d\boldsymbol{x} \\ &= \int_{\mathbb{R}^d} \left\{ \frac{1}{2}\left(|\nabla u(\boldsymbol{x})|^2 + |\nabla v(\boldsymbol{x})|^2\right) + (V + 2\beta|\phi_s|^2 + \lambda\Phi_s - \mu_s)(|u(\boldsymbol{x})|^2 + |v(\boldsymbol{x})|^2) \right. \\ &\quad \left. + \beta\left(\phi_s^2\bar{u}v + \bar{\phi}_s^2 u\bar{v}\right) + \lambda\left[\bar{u}\hat{\chi}_1(u) + \bar{v}\hat{\chi}_1^*(v) + \bar{u}\hat{\chi}_2(v) + \bar{v}\hat{\chi}_2^*(u)\right]\right\} d\boldsymbol{x}. \end{aligned} \tag{24}$$

∎

It is easy to check that the right-hand side of (24) is real, and hence substituting equation (24) from its conjugate, we arrive at the identity (23).

Remark 1. From this lemma, we note that under the normalization constraint (19) only the real eigenvalues for BdGEs are relevant for the elementary excitations. Complex eigenvalues, which play a crucial rule in determining the dynamical stability of stationary states, may occur for BdGEs (18) only if $\|u\| = \|v\|$. Now that we focus on the elementary excitation, i.e., BdGEs (18) with constraint (19), we reasonably assume ω is real throughout this paper and leave the study of complex eigenvalues of BdGEs as future work.

For harmonic potential $V(\boldsymbol{x}) = \frac{1}{2}\sum_\alpha \gamma_\alpha^2 \alpha^2$ with spatial variables $\alpha = x, y$ in two dimensions and $\alpha = x, y, z$ in three dimensions, we have the following results for the corresponding Bogoliubov excitations.

LEMMA 2. *Let ϕ_s be the real-valued stationary state of GPE* (1)*; then we have the following solution pair to the BdGEs* (18) *with constraint* (19)*:*

$$\{u_\alpha, v_\alpha, \omega_\alpha\} =: \left\{ \frac{1}{\sqrt{2}} \left(\gamma_\alpha^{-1/2} \partial_\alpha \phi_s - \gamma_\alpha^{1/2} \alpha \phi_s \right),\ \frac{1}{\sqrt{2}} \left(\gamma_\alpha^{-1/2} \partial_\alpha \phi_s + \gamma_\alpha^{1/2} \alpha \phi_s \right),\ \gamma_\alpha \right\},$$

with $\alpha = x, y$ in two dimensions and $\alpha = x, y, z$ in three dimensions.

Proof. Notice that stationary state ϕ_s satisfies the Euler–Lagrange equation (8); differentiating (8) with respect to variable x, we have

$$H_+(\partial_x \phi_s) = (-\frac{1}{2}\nabla^2 + V + 3\beta|\phi_s|^2 + \lambda\Phi_s + 2\lambda\hat{\chi}_1 - \mu_s)(\partial_x \phi_s) = \gamma_x(-\gamma_x x \phi_s).$$

Apply H_- on $-\gamma_x x$ and combine (8); we have

$$H_-(-\gamma_x x \phi_s) = (-\frac{1}{2}\nabla^2 + V + \beta|\phi_s|^2 + \lambda\Phi_s - \mu_s)(-\gamma_x x \phi_s) = \gamma_x(\partial_x \phi_s).$$

Therefore, it is clear that $(\partial_x \phi_s, -\gamma_x x \phi_s)$ solves (21) with $\omega = \gamma_x$. Noticing $-\int_{\mathbb{R}^2} \gamma_x x \phi_s \partial_x \phi_s \mathrm{d}x\mathrm{d}y = \frac{\gamma_x}{2}$, we conclude that $(f, g) = (\frac{1}{\sqrt{2}}\gamma_x^{-\frac{1}{2}} \partial_x \phi_s, -\frac{1}{\sqrt{2}}\gamma_x^{\frac{1}{2}} x \phi_s)$ solves (22) under the normalization constraint for $\omega = \gamma_x$. Using (20), we derive the following analytic solution:

$$\omega_x = \gamma_x, \quad u_x = \frac{1}{\sqrt{2}} \left(\gamma_x^{-\frac{1}{2}} \partial_x \phi_s - \gamma_x^{\frac{1}{2}} x \phi_s \right), \quad v_x = \frac{1}{\sqrt{2}} \left(\gamma_x^{-\frac{1}{2}} \partial_x \phi_s + \gamma_x^{\frac{1}{2}} x \phi_s \right).$$

The conclusion holds true for $\alpha = y, z$ following similar argument, and we omit the proof for brevity. ∎

In addition, in the Thomas–Fermi (TF) regime, i.e., $\beta \gg 1$, for dipolar BECs with dipoles lying along the z-axis, i.e., $\boldsymbol{n} = (0, 0, 1)^T$, and trapped by a cylindrically symmetric harmonic trapping potential $V(\boldsymbol{x})$, i.e., $\gamma_x = \gamma_y$ in (4), we have the following results for the ground state profile $\phi_g(\boldsymbol{x})$ and the corresponding Bogoliubov excitations.

LEMMA 3. *The ground state profile $\phi_g(\boldsymbol{x})$ of GPE* (10) *could be well approximated by the TF density $\phi_g^{\mathrm{TF}}(\boldsymbol{x})$ with chemical potential μ_g^{TF}* [22]:

$$\phi_g(\boldsymbol{x}) \approx \phi_g^{\mathrm{TF}}(\boldsymbol{x}) := \sqrt{\frac{15}{8\pi R^2 R_z} \left(1 - \frac{x^2}{R^2} - \frac{y^2}{R^2} - \frac{z^2}{R_z^2} \right)_+}.$$

Here, $\mu_g^{\rm TF} = \frac{15\,(\beta-\lambda\,\eta(\kappa))}{8\pi R^2 R_z}$ *is the chemical potential,* $f_+(\boldsymbol{x}) := \max\{0, f(\boldsymbol{x})\}$*, and*

$$\eta(\kappa) := \begin{cases} \dfrac{1+2\kappa^2}{1-\kappa^2} - \dfrac{3\kappa^2 \mathrm{arctanh}(\sqrt{1-\kappa^2})}{(1-\kappa^2)^{3/2}}, & \kappa \le 1, \\ \dfrac{1+2\kappa^2}{\kappa^2-1} - \dfrac{3\kappa^2 \arctan(\sqrt{\kappa^2-1})}{(\kappa^2-1)^{3/2}}, & \kappa > 1, \end{cases}$$

where the ratio $\kappa := R/R_z$ *is determined by the transcendental equation*

$$\frac{3\lambda\kappa^2}{\beta}\left[\left(\frac{\gamma_z^2}{2\gamma_x^2}+1\right)\frac{\eta(\kappa)}{1-\kappa^2}-1\right] + \left(\frac{\lambda}{\beta}-1\right)\left(\kappa^2 - \frac{\gamma_z^2}{\gamma_x^2}\right) = 0. \tag{25}$$

The radius R *is given explicitly as*

$$R = \left[\frac{15\kappa}{4\pi\gamma_x^2}\beta\left(1+\frac{\lambda}{\beta}\left(\frac{3\kappa^2\eta(\kappa)}{2(1-\kappa^2)}-1\right)\right)\right]^{\frac{1}{5}}. \tag{26}$$

Moreover, as $\beta \to \infty$*, we have the asymptotic results*

$$R = \mathcal{O}(\beta^{1/5}), \qquad R_z = \mathcal{O}(\beta^{1/5}), \qquad \mu_g^{\rm TF} = \mathcal{O}(\beta^{2/5}).$$

LEMMA 4. *Under the same conditions of Lemma* 3*, the Bogoliubov eigenvalues associated with* (13) *and* (14)*, denoted by* ω_β*, are well approximated by* ω_∞ *as* $\beta \to \infty$*. The limit eigenvalue* ω_∞ *satisfies*

$$-\left(1-\frac{1}{2}(\gamma_x^2x^2+\gamma_x^2y^2+\gamma_z^2z^2)\right)\nabla^2 q + (\gamma_x^2 x\partial_x + \gamma_y^2 y\partial_y + \gamma_z^2 z\partial_z)q = (\omega_\infty)^2 q(\boldsymbol{x})$$

for $\boldsymbol{x} \in D_\infty := \left\{\boldsymbol{x}\in\mathbb{R}^3 \middle| 1-\frac{1}{2}(\gamma_x^2x^2+\gamma_x^2y^2+\gamma_z^2z^2) \ge 0\right\}$*. Especially, for a special isotropic harmonic trap, i.e.,* $\gamma_x = \gamma_y = \gamma_z = \sqrt{2}$*, we have the explicit eigenvalues*

$$\omega_\infty^{l,k} = \sqrt{2}\sqrt{l+3k+2kl+2k^2}, \qquad l \ge 0, \quad k \ge 0.$$

Proof. To estimate the asymptotics of ω_β for large β, we first introduce the rescaling $\widetilde{\boldsymbol{x}} = \boldsymbol{x}/\sqrt{\mu_g}$ and $\phi_g(\boldsymbol{x}) = \sqrt{\frac{\mu_g}{\beta}}\widetilde{\phi}_g(\widetilde{\boldsymbol{x}})$, then we obtain the following formula:

$$\Phi_g(\boldsymbol{x}) = \frac{\mu_g}{\beta}\widetilde{\Phi}_g(\widetilde{\boldsymbol{x}}), \qquad \widetilde{\Phi}_g(\widetilde{\boldsymbol{x}}) := \left(U * |\widetilde{\phi_g}|^2\right)(\widetilde{\boldsymbol{x}}),$$
$$\left[\hat{\chi}(f)\right](\boldsymbol{x}) = \frac{\mu_g}{\beta}\left[\widetilde{\hat{\chi}}(\widetilde{f})\right](\widetilde{\boldsymbol{x}}), \qquad f(\boldsymbol{x}) = \widetilde{f}(\widetilde{\boldsymbol{x}}).$$

The second BdGE (22), i.e., $H_+H_-g = \omega^2 g$, is now rescaled as $\widetilde{H}_+\widetilde{H}_-\widetilde{g} = \frac{\omega^2}{\mu_g^2}\widetilde{g}$ with

$$\widetilde{H}_+ = -\frac{1}{2\mu_g^2}\widetilde{\nabla}^2 + \widetilde{V}(\widetilde{\boldsymbol{x}}) + 3|\widetilde{\phi}_g|^2 + \frac{\lambda}{\beta}\widetilde{\Phi}_g + 2\frac{\lambda}{\beta}\widetilde{\hat{\chi}} - 1, \qquad \widetilde{H}_- = \widetilde{H}_+ - 2|\widetilde{\phi}_g|^2 - 2\frac{\lambda}{\beta}\widetilde{\hat{\chi}}, \tag{27}$$

$\widetilde{\nabla}^2 = \frac{\partial^2}{\partial\widetilde{x}^2} + \frac{\partial^2}{\partial\widetilde{y}^2} + \frac{\partial^2}{\partial\widetilde{z}^2}$, and $\widetilde{V}(\widetilde{\boldsymbol{x}}) = \frac{1}{2}(\gamma_x^2\widetilde{x}^2 + \gamma_x^2\widetilde{y}^2 + \gamma_z^2\widetilde{z}^2)$. The eigenvalue problem (8) is then rescaled as

$$\left[-\frac{1}{2}\frac{1}{\mu_g^2}\widetilde{\nabla}^2 + \widetilde{V}(\widetilde{\boldsymbol{x}}) + |\widetilde{\phi}_g|^2 + \frac{\lambda}{\beta}\widetilde{\Phi}_g\right]\widetilde{\phi}_g = \widetilde{\phi}_g. \tag{28}$$

Combing (27) and (28), we have

$$\left[-\frac{1}{2\mu_g^2}\widetilde{\nabla}^2+\widetilde{V}(\widetilde{\boldsymbol{x}})+3|\widetilde{\phi}_g|^2+\frac{\lambda}{\beta}\widetilde{\Phi}_g+2\frac{\lambda}{\beta}\widetilde{\chi}-1\right]\left[-\frac{1}{2\mu_g^2}\widetilde{\nabla}^2+\frac{1}{2\mu_g^2}\frac{1}{\widetilde{\phi}_g}\widetilde{\nabla}^2\widetilde{\phi}_g\right]\widetilde{g}=\frac{\omega^2}{\mu_g^2}\widetilde{g}.$$

In the TF regime ($\beta\gg 1$), the rescaled $\widetilde{\phi}_g^{\mathrm{TF}}$ converges to $\widetilde{\phi}_g^{\infty}(\widetilde{\boldsymbol{x}})=(1-\frac{1}{2}(\gamma_x^2\widetilde{x}^2+\gamma_y^2\widetilde{y}^2+\gamma_z^2\widetilde{z}^2))_+^{\frac{1}{2}}$ as $\beta\to\infty$. In the above equation, by substituting $\widetilde{\phi}_g^{\mathrm{TF}},\widetilde{\mu}_g^{\mathrm{TF}}$ for the ground state $\widetilde{\phi}_g$ and the chemical potential μ_g, respectively, we obtain the following eigenvalue problem:

$$\left[\frac{-1}{2(\mu_g^{\mathrm{TF}})^2}\widetilde{\nabla}^2+\widetilde{V}(\widetilde{\boldsymbol{x}})+3|\widetilde{\phi}_g^{\mathrm{TF}}|^2-1\right]\left[-\frac{1}{2(\mu_g^{\mathrm{TF}})^2}\widetilde{\nabla}^2+\frac{1}{2(\mu_g^{\mathrm{TF}})^2}\frac{1}{\widetilde{\phi}_g^{\mathrm{TF}}}\widetilde{\nabla}^2\widetilde{\phi}_g^{\mathrm{TF}}\right]\widetilde{g}\approx\frac{\omega^2}{(\mu_g^{\mathrm{TF}})^2}\widetilde{g}.$$

When $\beta\to\infty$, by plugging in the limit function $\widetilde{\phi}_g^{\infty}$ and dropping the higher order term of $1/\mu_g^{\mathrm{TF}}$, we derive the limit eigenvalue problem for $q=\widetilde{g}/\widetilde{\phi}_g^{\mathrm{TF}}$ as follows:

$$(29)-\left(1-\frac{1}{2}(\gamma_x^2\widetilde{x}^2+\gamma_x^2\widetilde{y}^2+\gamma_z^2\widetilde{z}^2)\right)\widetilde{\nabla}^2q+(\gamma_x^2\widetilde{x}\partial_{\widetilde{x}}+\gamma_y^2\widetilde{y}\partial_{\widetilde{y}}+\gamma_z^2\widetilde{z}\partial_{\widetilde{z}})q=\omega_\infty^2q(\widetilde{\boldsymbol{x}}).$$

Especially, when $\gamma_x=\gamma_y=\gamma_z=\sqrt{2}$, $q(\boldsymbol{x})$ is spherically symmetric, (29) could be solved explicitly in a similar way as shown in [34]. ∎

3. Numerical method. In this section, we will propose efficient and spectral-accurate numerical methods to solve the BdGEs (18) with constraint (19). Due to the external trapping potential $V(\boldsymbol{x})$, the wave function $\psi(\boldsymbol{x})$, and the ground/stationary states $\phi_s(\boldsymbol{x})$ to the GPE (1)–(3), as well as the eigenfunctions $(u(\boldsymbol{x}),v(\boldsymbol{x}))$ to the BdGEs (18) and (19), are all smooth and fast decaying. Therefore, it is reasonable to truncate the whole space $\mathbb{R}^d$ into a bounded domain $\mathcal{D}\subset\mathbb{R}^d$ with periodic boundary conditions such that the truncation error is negligible. To numerically solve the BdGEs, high spatial resolution schemes are usually preferred. In terms of accuracy, simplicity, and efficiency, the Fourier pseudospectral (FS) discretization [9, 10, 11] is one of the most optimal candidates. However, due to the polynomially decaying properties (at the far field $|\boldsymbol{x}|\to\infty$) of the convolution-type nonlocal potentials Φ_s (15) and the nonlocal interaction $\chi_j(\xi)$ (17) , the FS scheme could not be directly applied. Indeed, it is the most challenging job to compute such nonlocal interactions with spectral accuracy as efficiently as possible. Alternative spectral-accurate solvers, such as the kernel truncation method [47] and nonuniform fast Fourier transform method [13, 31], usually require prohibitively huge memory and/or expensive computational cost, thus bottlenecking the overall efficiency. In this section, we will propose a spectral-accurate solver to evaluate such nonlocal interactions via direct FS discretizations with minimal storage and optimal efficiency; then the full FS scheme for the BdGEs (18) achieves both optimal accuracy and efficiency.

3.1. Space discretization and eigensystem solver. We first introduce the FS scheme [9, 10, 11] to discretize the BdGEs (18) provided that the stationary state ϕ_s is computed accurately by the PCG method [4, 5, 45] and the DDI potential Φ_s can be easily evaluated by the SFSC method, which is to be introduced in next section. For simplicity, we only present the scheme for the 2D case. We choose the computation domain $\mathcal{D}$ as a square for simplicity and denote it by $\mathcal{D}_L:=[-L,L]\times[-L,L]$. Let N

and M be two positive even integers. Choose $h_x = \frac{2L}{N}$ and $h_y = \frac{2L}{M}$ as the mesh size in x- and y-directions, respectively. Define the indices and grid point sets as

$$\mathcal{I}_{NM} = \Big\{(n,m) \in \mathbb{N}^2 \,|\, 0 \le n \le N-1,\ 0 \le m \le M-1\Big\},$$
$$\widetilde{\mathcal{I}}_{NM} = \Big\{(\ell,k) \in \mathbb{Z}^2 \,|\, -N/2 \le \ell \le N/2-1,\ -M/2 \le k \le M/2-1\Big\},$$
$$\mathcal{T}_{\boldsymbol{x}} = \Big\{(x_n,\, y_m) =: (-L + n\,h_x,\ -L + m\,h_y), \quad (n,m) \in \mathcal{I}_{NM}\Big\},$$

and introduce the functions

$$W_{\ell k}(x,y) = e^{i\mu_\ell^x (x+L)} e^{i\mu_k^y (y+L)}, \quad (\ell,k) \in \widetilde{\mathcal{I}}_{NM}, \tag{30}$$

with $\mu_\ell^x = \frac{2\pi\ell}{2L}$ and $\mu_k^y = \frac{2\pi k}{2L}$. Moreover, we define $P_{nm} =: P(x_n, y_m)$ ($P = u, v, \phi_s, \Phi_s$, etc.) as the value of an abstract function $P(x,y)$ at grid $(x_n, y_m) \in \mathcal{T}_{\boldsymbol{x}}$ and $\boldsymbol{P}$ as the vector with components $\{P_{nm}\}$. The FS approximation of P (denoted by $\widetilde{P}$) and $\nabla^2 P$ reads as

$$P(x,y) \approx \widetilde{P}(x,y) := \sum_{\ell=-N/2}^{N/2-1} \sum_{k=-M/2}^{M/2-1} \widehat{\boldsymbol{P}}_{\ell k}\, W_{\ell k}(x,y), \tag{31}$$

$$(\nabla^2 P) \approx (\nabla^2 \widetilde{P}) := \sum_{\ell=-N/2}^{N/2-1} \sum_{k=-M/2}^{M/2-1} -\Big((\mu_\ell^x)^2 + (\mu_k^y)^2\Big)\, \widehat{\boldsymbol{P}}_{\ell k}\, W_{\ell k}(x,y), \tag{32}$$

where $\widehat{\boldsymbol{P}} \in \mathbb{C}^{NM}$, the discrete Fourier transform coefficient of $\boldsymbol{P}$, is computed as

$$\widehat{\boldsymbol{P}}_{\ell k} = \frac{1}{NM} \sum_{n=0}^{N-1} \sum_{m=0}^{M-1} P_{nm}\, \overline{W}_{\ell k}(x_n, y_m), \qquad (\ell,k) \in \widetilde{\mathcal{I}}_{NM}. \tag{33}$$

The nonlocal operators $\widehat{\chi}_j$ and $\widehat{\chi}_j^*$ ($j = 1, 2$) are approximated, respectively, as

$$(\widehat{\chi}_j P)(x,y) \approx (\widehat{\chi}_j \widetilde{P})(x,y), \qquad (\widehat{\chi}_j^* P)(x,y) \approx (\widehat{\chi}_j^* \widetilde{P})(x,y), \qquad (x,y) \in \mathcal{D},$$

and the operators $\mathcal{L}_{\rm GP}$ and $\mathcal{L}_{ij}$ ($i,j = 1,2$) in (16) are then discretized at $\boldsymbol{x}_{nm} := (x_n, y_m) \in \mathcal{T}_{\boldsymbol{x}}$ as follows:

$$(\mathcal{L}_{\rm GP} P)(\boldsymbol{x}_{nm}) \approx -\frac{1}{2}(\nabla^2 \widetilde{P})(\boldsymbol{x}_{nm}) + (V_{nm} + \beta|(\phi_s)_{nm}|^2 + \lambda(\Phi_s)_{nm} - \mu_s)\widetilde{P}(\boldsymbol{x}_{nm}),$$
$$(\mathcal{L}_{ij} P)(\boldsymbol{x}_{nm}) \approx (\mathcal{L}_{ij} \widetilde{P})(\boldsymbol{x}_{nm}) := (\mathbf{L}_{ij}\mathbf{P})_{nm}.$$

The BdGEs (18) with constraint (19) then could be discretized into the linear algebraic system

$$\begin{pmatrix} \mathbf{L}_{11} & \mathbf{L}_{12} \\ \mathbf{L}_{21} & \mathbf{L}_{22} \end{pmatrix} \begin{pmatrix} \boldsymbol{u} \\ \boldsymbol{v} \end{pmatrix} = \omega \begin{pmatrix} \boldsymbol{u} \\ \boldsymbol{v} \end{pmatrix}, \qquad h_x h_y \Big(\|\boldsymbol{u}\|^2 - \|\boldsymbol{v}\|^2\Big) = 1, \tag{34}$$

with $\|\cdot\|$ being the standard l^2 norm.

Then we describe the approach to solve the discrete BdGEs (34) briefly. First, the stationary state ϕ_s and chemical potential μ_s (34) are precomputed via the PCG method [4, 45] in a large enough domain with small enough mesh size such that the errors coming from this evaluation are negligible. The values of ϕ_s on grid points

$\mathcal{T}_{\boldsymbol{x}}$ are interpolated by the Fourier spectral method. The involved nonlocal potentials/operators, such as Φ_s and $\widehat{\chi}_j (j = 1, 2)$, are evaluated by the nonlocal solver to be introduced in next section. Second, we solve the linear eigenvalue/vector problem (34). In practice, the IRAM [42] is adapted to simultaneously compute the first few smallest positive eigenvalues ω and their associated eigenvectors $(\boldsymbol{u}, \boldsymbol{v})$ followed by a rescaling in order to meet the normalization constraint. One important note is that the matrix of (34) is nonsymmetric and dense; therefore explicit matrix representation requires expensive memory storage. This would notably bottleneck the efficiency if one directly applies the IRAM, especially for the 3D problems. Hence, it is essential and necessary to utilize the matrix-free version of the IRAM, which could be well resolved by coding with the well-known ARPACK [46] library. In such case, all that one needs is to provide the matrix-vector product (operator-function action on the continuous level), that is, to compute $\mathbf{L}_{i1}\boldsymbol{u}^p + \mathbf{L}_{i2}\boldsymbol{v}^p$, where vectors $\boldsymbol{u}^p, \boldsymbol{v}^p \in \mathbb{C}^{NM}$ are updated iteratively.

The discrete Fourier transform and its inverse (31)–(33) could be computed efficiently via the FFT and inverse FFT (iFFT) within $O(NM \log(NM))$ operations. All the other operators in $\mathcal{L}_{ij}$ except the nonlocal interaction $\widehat{\chi}_j$ are in fact multiplication operators in the physical space; thus their operations on $\boldsymbol{u}$ and $\boldsymbol{v}$ could be easily accessed by pointwise function multiplication. The nonlocal interaction consists of convolution and function multiplication; therefore, it is not diagonalizable in either phase or physical space, which bottlenecks the overall efficiency as well as the accuracy. Therefore, the efficient and accurate evaluation of the nonlocal potentials is of essential importance in solving the BdGEs. In next subsection, we shall propose a *simple Fourier spectral convolution* (SFSC) algorithm, which could optimally evaluate such nonlocal interactions with spectral accuracy within $O(NM \log(NM))$ operations.

3.2. SFSC method for the nonlocal interactions. It is clear that all the nonlocal interactions are composed of convolution and function multiplication. The multiplication with the stationary state ϕ_s (or its conjugate) is quite straightforward; thus we concentrate on the convolution in this subsection. Without loss of generality, we consider $\varphi := U * (\phi_s f)$ with f being smooth and fast decaying on the same computational domain $\mathcal{D}$. The kernel U is singular at the origin and decays polynomially at the far field, and the density $\rho := \phi_s f$ is smooth and fast decaying too. The convolution evaluation is quite challenging in terms of both accuracy and efficiency, even though it can be transformed to Coulomb potential $(U(\boldsymbol{x}) = 1/(2\pi|\boldsymbol{x}|))$. For example, the convolution can be equivalently rewritten as

$$\varphi = \left(\frac{1}{2\pi|\boldsymbol{x}|}\right) * \left(-\frac{3}{2}(\partial_{n_\perp n_\perp} - n_3^2\nabla_\perp^2)\rho\right) := \left(\frac{1}{2\pi|\boldsymbol{x}|}\right) * \widetilde{\rho}, \tag{35}$$

where $\widetilde{\rho}$ is the effective DDI-density for the 2D Coulomb potential. The 3D convolution can also be transformed to Coulomb potential with similar kernel $U(\boldsymbol{x}) = 1/(4\pi|\boldsymbol{x}|)$, and we omit details for brevity.

To simplify the presentation, we assume the computational domain $\mathcal{D} = \mathcal{D}_L := \prod_{j=1}^{d}[-L, L]$ is a cube centered at the origin of length $2L$ in each spatial direction. Existing convolution solvers either require extra zero-padding [47] or perform inefficiently in higher spatial dimensions [31, 13]. We now propose an efficient approach which requires optimal two-fold zero-padding and is easily implemented with FFT/iFFT. To be exact, we take the following 2D case as an example.

For simplicity's sake, we replace $\widetilde{\rho}$ by ρ and assume further that the density is compactly supported (numerically) in $\mathcal{D}_L$. To compute the interaction at $\boldsymbol{x} \in \mathcal{D}_L$, we have

$$\varphi(\boldsymbol{x}) = \int_{\mathbb{R}^2} U(\boldsymbol{y})\rho(\boldsymbol{x}-\boldsymbol{y})\mathrm{d}\boldsymbol{y}, \quad \boldsymbol{x} \in \mathcal{D}_L, \tag{36}$$

$$= \int_{\boldsymbol{x}+\mathcal{D}_L} U(\boldsymbol{y})\rho(\boldsymbol{x}-\boldsymbol{y})\mathrm{d}\boldsymbol{y} = \int_{\mathcal{D}_{2L}} U(\boldsymbol{y})\rho(\boldsymbol{x}-\boldsymbol{y})\mathrm{d}\boldsymbol{y}. \tag{37}$$

For $\boldsymbol{x} \in \mathcal{D}_L$, the whole space domain $\mathbb{R}^2$ is reduced to $\boldsymbol{x}+\mathcal{D}_L$ because $\rho(\boldsymbol{x}-\boldsymbol{y}) = 0 \,\forall\, \boldsymbol{y} \notin \boldsymbol{x}+\mathcal{D}_L$, and the third equation holds true as the density is compactly supported (numerically) in $\mathcal{D}_L$. Therefore, we have $\boldsymbol{x}-\boldsymbol{y} \in \mathcal{D}_{3L} \;\forall\; \boldsymbol{x} \in \mathcal{D}_L,\ \boldsymbol{y} \in \mathcal{D}_{2L}$. Then we need to approximate the density ρ on $\mathcal{D}_{3L}$. However, with careful investigation on the periodicity of Fourier basis, it suffices to approximate ρ on a two-fold domain $\mathcal{D}_{2L}$, and we refer to [21] for details. After a two-fold zero-padding of the density ρ, we obtain the Fourier series approximation on $\mathcal{D}_{2L}$ as

$$\rho(\boldsymbol{z}) \approx \sum_{p=-N}^{N-1}\sum_{q=-M}^{M-1} \widehat{\rho}_{pq}\ \ e^{i\widetilde{\mu}_p^x(x+2L)}e^{i\widetilde{\mu}_q^y(y+2L)}, \quad \boldsymbol{z} := (x,y) \in \mathcal{D}_{2L}, \tag{38}$$

with $\widetilde{\mu}_p^x = \pi p/(2L), \widetilde{\mu}_q^y = \pi q/(2L)$, and $\widehat{\rho}_{pq}$ being the discrete Fourier transform. Plugging (38) into (37) and substituting $\boldsymbol{x}-\boldsymbol{y}$ for $\boldsymbol{z}$, we have

$$\varphi(\boldsymbol{x}) \approx \sum_{p=-N}^{N-1}\sum_{q=-M}^{M-1} \widehat{\rho}_{pq}\ \widehat{U}_{pq}\ \ e^{i\widetilde{\mu}_p^x(x+2L)}e^{i\widetilde{\mu}_q^y(y+2L)}, \qquad \boldsymbol{x} \in \mathcal{D}_L, \tag{39}$$

where $\widehat{U}_{pq} =: \widehat{U}(\widetilde{\mu}_p^x, \widetilde{\mu}_q^y)$ is the Fourier transform of U on bounded domain $\mathcal{D}_{2L}$, which is given explicitly as follows:

$$\widehat{U}_{pq} = \int_{\mathcal{D}_{2L}} U(\boldsymbol{x})\ e^{-i\widetilde{\mu}_p^x x}e^{-i\widetilde{\mu}_q^y y}\mathrm{d}\boldsymbol{x} = (2L)\int_{\mathcal{D}_1} U(\boldsymbol{x})\ e^{-i\pi p x}e^{-i\pi q y}\mathrm{d}\boldsymbol{x}. \tag{40}$$

The last equation holds with a change of variables $\boldsymbol{x} = 2L\widetilde{\boldsymbol{x}}$ for the Coulomb potential. The Fourier transform $\widehat{U}_{pq}$ can be reduced to a singular Fourier integral on the standard domain $\mathcal{D}_1 = [-1,1]^2$ and can be precomputed very accurately up to machine precision via some high-precision library such as the Advanpix toolbox [1]. If $\widehat{U}_{pq}$ is to be computed on the fly, we recommend the Gaussian-summation acceleration techniques [25]. Once (40) is available, the Coulomb potential on $\mathcal{T}_{\boldsymbol{x}}$ can be computed with one pair FFT/iFFT and one function multiplication of size $4NM$, and the overall cost is $O(4NM + 4NM\log(4NM))$. Note that the potential φ on mesh; $\mathcal{T}_{\boldsymbol{x}}$, which is a uniform partition of $\mathcal{D}_L$, is part of the inverse FFT (on a two-fold zero-padded mesh); therefore, no interpolation is ever needed at this step. The efficiency is almost optimal compared with existing methods, and the accuracy achieved is close to machine precision as expected.

To summarize, the nonlocal interaction $\widehat{\chi}_j(f)$ ($\widehat{\chi}_j^*(f)$) can be computed efficiently in two steps: (i) compute the convolution with density $\phi_s f$ ($\bar{\phi}_s f$) (ii) multiply the interaction φ and the ground state ϕ_s ($\bar{\phi}_s$). We present a detailed step-by-step algorithm using $\widehat{\chi}_1(f)$ as an example, and adaptation to $\widehat{\chi}_2(f)$ and $\widehat{\chi}_j^*(f)$ is straightforward. The algorithm to compute the nonlocal interaction is summarized in Algorithm 1.

Algorithm 1 SFSC for $\widehat{\chi}_1(f)$

Comment: Given a smooth function f, ground state ϕ_s, and DDI Φ_s on mesh grid $\mathcal{T}_{\boldsymbol{x}}$.

Comment: Precompute the Fourier transform $\widehat{U}_{pq}$ (40) up to controlled tolerance ϵ.

1: Compute density $\rho =: \phi_s f$ by multiplication.
2: Compute the effective DDI-density $\widetilde{\rho}$ (35) by differentiating ρ on $\mathcal{T}_{\boldsymbol{x}}$ via the Fourier spectral method.
3: Carry out a two-fold zero-padding of DDI-density (denoted by $\widetilde{\rho}$).
4: Compute the discrete Fourier coefficient of $\widetilde{\rho}$ via FFT, i.e., $\widehat{\rho}_{pq}$ in (38).
5: Compute $\widehat{\rho}_{pq}\widehat{U}_{pq}$ by multiplication.
6: Compute the nonlocal potential φ (39) on $\mathcal{T}_{\boldsymbol{x}}$ via iFFT.
7: Compute $\chi_1(f) = \varphi\phi_s$ by multiplication.

To show the accuracy and efficiency, we carry out the following example. For simplicity, we only evaluate nonlocal interaction $\chi_1(f)$ in two and three dimensions. Unless stated otherwise, we let

$$f(\boldsymbol{x}) = e^{-\frac{|\boldsymbol{x}|^2}{2\sigma^2}}, \qquad \phi_s(\boldsymbol{x}) = f(\boldsymbol{x}), \qquad \boldsymbol{x} \in \mathbb{R}^d \tag{41}$$

and set the dipole orientation as $\boldsymbol{n} = (0.82778, 0.41505, -0.37751)^T$. We set the computational domain as $\mathcal{D} = [-8, 8]^d$, and we always use uniform (tensor) grids in space with equal mesh sizes h in all directions. To quantify the errors, we define the error function as

$$E_h =: \frac{\left\|[\chi_1(f)]_{\text{num}} - [\chi_1(f)]_{\text{exact}}\right\|_\infty}{\left\|[\chi_1(f)]_{\text{exact}}\right\|_\infty},$$

where $[\chi_1(f)]_{\text{num}}$ is the numerical solution obtained by SFSC and $[\chi_1(f)]_{\text{exact}}$ is the exact solution.

Example 1. With the choice of f and ϕ_s in (41), the exact interaction $\chi_1(f)$ in two dimensions can be given explicitly as

$$\begin{aligned}\chi_1(f)(\boldsymbol{x}) = {} & \frac{3\sqrt{\pi}e^{-s}}{4\sigma}\left[(\boldsymbol{n}_\perp\cdot\boldsymbol{n}_\perp)(I_0(s)-I_1(s)) - \frac{2(\boldsymbol{x}\cdot\boldsymbol{n}_\perp)^2}{\sigma^2}\Big(I_0(s)-\frac{1+2s}{2s}I_1(s)\Big)\right]f(\boldsymbol{x}) \\ & + \frac{3\sqrt{\pi}\,n_3\,n_3\,s\,e^{-s}}{\sigma}\Big[I_0(s) - I_1(s) - \frac{I_0(s)}{2\,s}\Big]f(\boldsymbol{x}),\end{aligned}$$

where $s = \frac{|\boldsymbol{x}|^2}{2\sigma^2}$ and I_0 and I_1 are the modified Bessel functions of order 0 and 1, respectively. While in three dimensions, we have

$$\chi_1(f)(\boldsymbol{x}) = -\left[\rho(\boldsymbol{x}) + 3\,\partial_{\boldsymbol{nn}}\left(\frac{\sigma^2\sqrt{\pi}}{4}\frac{\mathrm{Erf}(r/\sigma)}{r/\sigma}\right)\right]f(\boldsymbol{x}) = -[\rho(\boldsymbol{x}) + 3\,\boldsymbol{n}^T B(\boldsymbol{x})\boldsymbol{n}]f(\boldsymbol{x}) \tag{42}$$

with matrix $B(\boldsymbol{x}) = (b_{jl}(\boldsymbol{x}))_{j,l=1}^3$ defined as

$$b_{jl}(\boldsymbol{x}) = \left(\frac{\sigma^2}{2r^2}e^{-\frac{r^2}{\sigma^2}} - \frac{\sigma^3\sqrt{\pi}}{4r^3}\mathrm{Erf}\left(\frac{r}{\sigma}\right)\right)\delta_{jl} \tag{43}$$

$$+x_j x_l\left(-e^{-\frac{r^2}{\sigma^2}}\left(\frac{3\,\sigma^2}{2\,r^4} + \frac{1}{r^2}\right) + \frac{3\sigma^3\sqrt{\pi}}{4\,r^5}\mathrm{Erf}\left(\frac{r}{\sigma}\right)\right), \tag{44}$$

TABLE 1
Errors and CPU time (in seconds) for computing the nonlocal interaction $\chi_1(f)$ by SFSC with different mesh size h in 2D (upper) and 3D (lower) cases in Example 1.

	$h = 2$	$h = 1$	$h = 1/2$	$h = 1/4$
E_h	1.9385E−01	1.1617E−02	7.6144E−08	3.7585E−15
E_h	1.5743E−01	8.2904E−03	1.7048E−07	1.8485E−14
CPU	6.0000E−04	5.5000E−03	5.6300E−02	9.5620E−01

where $r = |\boldsymbol{x}|$, δ_{jl} is the Kronecker delta, $\boldsymbol{x} = (x_1, x_2, x_3)^T$, and $\mathrm{Erf}(r) = \frac{2}{\sqrt{\pi}} \int_0^r e^{-t^2} dt$ is the error function.

For all numerical examples in this paper, the related algorithms were implemented in Fortran and run on a 2.27 GHz Intel(R) Xeon(R) CPU E5520 with a 8 MB cache in Debian GNU/Linux. Table 1 shows the numerical errors E_h and corresponding CPU times by SFSC with different mesh size h for Example 1. Since the CPU time for the 2D case is too small, we only present those for the 3D case. From the table, we could clearly see that SFSC is efficient and achieves spectral accuracy.

4. Numerical results. In this section, we first test the convergence of the matrix-free IRAM integrated with the SFSC (SFSC-IRAM) method to solve the BdGEs (18). Then, we apply the SFSC-IRAM to investigate the Bogoliubov excitations around the ground states of GPEs. The ground state ϕ_s and chemical potential μ_s (34) are computed via the PCG-ATKM [45] in a large enough domain with a small enough mesh size such that the errors coming from spatial discretization are negligible. Unless stated otherwise, we choose the potential $V(\boldsymbol{x})$ as the harmonic trapping potential (4) and set, respectively, the computational domain as $\mathcal{D} = [-12, 12]^2$ in two dimensions and $\mathcal{D} = [-10, 10]^3$ in three dimensions. We always use uniform (tensor) grids in space with equal mesh sizes h in all directions.

4.1. Accuracy tests. Here, we first test the spatial accuracy of our method in two and three dimensions. To this end, we take the same parameters as in the Lemma 2, which imply an analytical formula for the eigenvalue and eigenvectors to the BdGEs (34). For an abstract analytical eigenvalue solution ω with multiplicity p to the BdGEs (34), we denote its associated analytical eigenvectors (as given in (25)) as $(\boldsymbol{u}_j, \boldsymbol{v}_j)$ $(j = 1, \ldots, p)$ and denote the corresponding linear eigenvector space as $P_u =: \mathrm{span}\{\boldsymbol{u}_1, \ldots, \boldsymbol{u}_p\}$ and $P_v =: \mathrm{span}\{\boldsymbol{v}_1, \ldots, \boldsymbol{v}_p\}$. For example, as shown in Lemma 2, for $\gamma_x = \gamma_y = \gamma$ in two dimensions, $p = 2$ for eigenvalue $\omega = \gamma$, and the associated eigenvectors $(\boldsymbol{u}_j, \boldsymbol{v}_j)$ $(j = 1, 2)$ are analytically given in (25). To demonstrate the results, we define the following error functions for eigenvalues and eigenvectors:

$$e^h_{\omega_\alpha} := \frac{|\omega^h_\alpha - \omega_\alpha|}{|\omega_\alpha|}, \qquad e^{h,\alpha}_{\boldsymbol{uv}} := \frac{\|\boldsymbol{u}^h_\alpha - \mathcal{P}_u \boldsymbol{u}^h_\alpha\|_2}{\|\boldsymbol{u}^h_\alpha\|_2} + \frac{\|\boldsymbol{v}^h_\alpha - \mathcal{P}_v \boldsymbol{v}^h_\alpha\|_2}{\|\boldsymbol{v}^h_\alpha\|_2}.$$

Here, with $\alpha = x, y$ in two dimensions and $\alpha = x, y, z$ in three dimensions, $\|\cdot\|_2$ is the discrete l^2 norm, and $\mathcal{P}_\nu$ $(\nu = u, v)$ is the l^2-orthogonal projection operator into space P_ν. $\{\boldsymbol{u}^h_\alpha, \boldsymbol{v}^h_\alpha, \omega^h_\alpha\}$ is the numerical approximation for the eigenpair $\{\boldsymbol{u}_\alpha, \boldsymbol{v}_\alpha, \omega_\alpha\}$ that is defined by (25) in Lemma 2.

Example 2. Here, we consider both the 2D and 3D examples. To this end, we set $\beta = 100$ and $\lambda = 50$ and consider the following four cases.

Case I. 2D case: Let $\gamma_x = \gamma_y = 1$ and $\boldsymbol{n} = (\cos\theta, \sin\theta, 0)^T$ with a different θ.
Case II. 2D case: Let $\gamma_x = \gamma_y/2 = 1$ and $\boldsymbol{n} = (\cos\theta, \sin\theta, 0)^T$ with a different θ.
Case III. 3D case: Let $\gamma_x = \gamma_y = \gamma_z = 1$ and $\boldsymbol{n} = (0, 0, 1)^T$.
Case IV. 3D case: Let $\gamma_x = \gamma_z = \gamma_y/2 = 1$ and $\boldsymbol{n} = (0, 0, 1)^T$.

For Case I, the two analytical eigenvalues are $\omega_x = \omega_y =: \omega = 1$; hence $p = 2$ for eigenvalue $\omega = 1$ and for the dimensions of its generated eigenvector spaces P_u and P_v. While $\omega_x = 1$ and $\omega_y = 2$ for Case II, both of their corresponding eigenvector spaces are of dimension one. Similarly, for Case III, the three analytical eigenvalues are $\omega_x = \omega_y = \omega_z =: \omega = 1$; hence $p = 3$ for eigenvalue $\omega = 1$ and for the dimensions of its associated eigenvector spaces P_u and P_v. For Case IV, $\omega_x = \omega_y =: \omega = 1$ and $\omega_z = 2$; thus the dimension of the associated eigenvector space is two for ω and one for ω_z, respectively.

Tables 2 and 3 illustrate the errors of eigenvalues and eigenvectors for different mesh size h and/or different dipole orientation $\boldsymbol{n}$ for Case I–Case IV. From this table, we could clearly see that the proposed method is of spectral accuracy in space.

4.2. Applications. In this section, we show some applications of the SFSC-IRAM to compute the Bogoliubov excitations around the ground state of the GPE with different parameters in two and three dimensions. We investigate the effect of

TABLE 2
Errors of the eigenvalues/eigenvectors for Case I *(upper) and Case* II *(lower) in Example* 2.

	h	$h_0 = 3/2$	$h_0/2$	$h_0/4$	$h_0/8$	$h_0/16$
$\theta = 0$	$e^h_{\omega_x}$	1.569E−01	6.618E−04	7.652E−07	1.516E−12	1.129E−11
	$e^h_{\omega_y}$	9.973E−02	1.927E−03	6.508E−08	7.641E−13	1.129E−11
	$e^{h,\omega_x}_{\boldsymbol{uv}}$	1.993E−01	1.211E−02	2.144E−04	3.474E−08	6.107E−11
	$e^{h,\omega_y}_{\boldsymbol{uv}}$	2.068E−01	1.932E−02	2.715E−05	4.611E−09	3.938E−11
$\theta = \pi/4$	$e^h_{\omega_x}$	2.085E−01	6.525E−04	3.957E−07	1.451E−13	5.653E−12
	$e^h_{\omega_y}$	1.283E−01	1.682E−03	1.967E−07	5.680E−13	1.299E−11
	$e^{h,\omega_x}_{\boldsymbol{uv}}$	1.851E−01	1.644E−02	1.214E−04	8.606E−09	3.962E−11
	$e^{h,\omega_y}_{\boldsymbol{uv}}$	2.989E−01	1.657E−02	1.325E−04	8.822E−09	5.275E−11
$\theta = \pi/3$	$e^h_{\omega_x}$	1.889E−01	7.926E−04	1.375E−07	4.345E−13	1.637E−11
	$e^h_{\omega_y}$	1.209E−01	3.174E−03	1.234E−06	1.217E−12	7.761E−12
	$e^{h,\omega_x}_{\boldsymbol{uv}}$	1.848E−01	1.490E−02	7.475E−05	1.851E−08	6.890E−11
	$e^{h,\omega_y}_{\boldsymbol{uv}}$	2.775E−01	1.779E−02	1.679E−04	1.873E−08	2.595E−11
	h	$h_0 = 3/4$	$h_0/2$	$h_0/4$	$h_0/8$	$h_0/16$
$\theta = 0$	$e^h_{\omega_x}$	1.583E−01	2.000E−03	2.131E−06	4.209E−12	1.220E−11
	$e^h_{\omega_y}$	1.858E−02	5.973E−03	1.388E−05	9.854E−13	9.976E−12
	$e^{h,\omega_x}_{\boldsymbol{uv}}$	4.431E−01	2.076E−02	2.421E−04	8.561E−08	5.781E−11
	$e^{h,\omega_y}_{\boldsymbol{uv}}$	2.000	7.879E−02	8.098E−04	8.165E−08	5.241E−11
$\theta = \pi/4$	$e^h_{\omega_x}$	2.168E−01	3.823E−03	3.399E−06	1.854E−11	1.004E−11
	$e^h_{\omega_y}$	1.215E−01	3.346E−02	1.104E−04	4.233E−10	3.712E−12
	$e^{h,\omega_x}_{\boldsymbol{uv}}$	5.428E−01	2.272E−02	1.931E−04	4.903E−08	1.565E−10
	$e^{h,\omega_y}_{\boldsymbol{uv}}$	2.000	1.022E−01	2.049E−03	1.910E−06	1.962E−10
$\theta = \pi/3$	$e^h_{\omega_x}$	2.251E−01	3.529E−04	7.674E−06	2.561E−11	4.069E−12
	$e^h_{\omega_y}$	1.553E−01	5.355E−03	1.755E−04	1.225E−09	6.111E−13
	$e^{h,\omega_x}_{\boldsymbol{uv}}$	4.452E−01	2.279E−02	1.768E−04	6.936E−08	5.168E−10
	$e^{h,\omega_y}_{\boldsymbol{uv}}$	2.000	1.014E−01	2.808E−03	3.584E−06	5.872E−11

TABLE 3
Errors of the eigenvalue/eigenvector for Case III *(upper) and Case* IV *(lower) in Example* 2.

	$h_0 = 4/5$	$h_0/2$	$h_0/4$	$h_0/8$
$e^h_{\omega_x}$	3.948E−02	2.623E−04	3.119E−11	4.456E−11
$e^h_{\omega_y}$	1.564E−02	1.463E−05	2.832E−11	1.334E−12
$e^h_{\omega_z}$	1.564E−02	1.463E−05	1.402E−09	9.087E−12
$e^{h,\omega_x}_{\boldsymbol{uv}}$	1.502E−01	5.478E−03	2.628E−07	6.311E−10
$e^{h,\omega_y}_{\boldsymbol{uv}}$	1.356E−01	2.047E−03	2.628E−07	1.753E−10
$e^{h,\omega_z}_{\boldsymbol{uv}}$	1.356E−01	2.047E−03	2.628E−07	1.753E−10
	$h_0 = 3/2$	$h_0/2$	$h_0/4$	$h_0/8$
$e^h_{\omega_x}$	1.256E−01	1.323E−03	2.963E−08	3.394E−10
$e^h_{\omega_y}$	1.049E−02	6.551E−03	1.885E−06	2.984E−11
$e^h_{\omega_z}$	1.704E−02	4.007E−04	2.352E−07	4.285E−11
$e^{h,\omega_x}_{\boldsymbol{uv}}$	3.592E−01	1.105E−02	1.216E−05	1.349E−09
$e^{h,\omega_y}_{\boldsymbol{uv}}$	2.000	1.240E−01	5.009E−04	8.537E−09
$e^{h,\omega_z}_{\boldsymbol{uv}}$	2.660E−01	1.616E−02	6.010E−05	3.409E−10

trapping potential, dipole orientation, and local/nonlocal interaction strength on the solutions to BdGEs. To this end, we fix $h = 1/8$ and study the following examples in two and three dimensions. We will only illustrate the results for the first few smallest positive eigenvalues and the associated eigenvectors.

Example 3. Here, we consider the effect of the interaction strength on the eigenvalues of the BdGEs with symmetric/asymmetric harmonic potentials in two dimensions. To this end, we study the following four cases.

Case I. Let $\gamma_x = \gamma_y = 1$, $\beta = 500$, and $\boldsymbol{n} = (0, 0, 1)^T$. Vary λ from -400 to 0.

Case II. Let $\gamma_x = \gamma_y = 1$, $\lambda = -100$, and $\boldsymbol{n} = (0, 0, 1)^T$. Vary β from 0 to 400.

Case III. Let $\gamma_x = 1$, $\gamma_y = \pi$, $\beta = 500$, and $\boldsymbol{n} = (1, 0, 0)^T$. Vary λ from 0 to 800.

Case IV. Let $\gamma_x = 1$, $\gamma_y = \pi$, $\lambda = 100$, and $\boldsymbol{n} = (1, 0, 0)^T$. Vary β from 0 to 800.

Figure 1 shows the nine smallest positive eigenvalues ω_ℓ ($\ell = 1, \ldots, 9$) for Case I–Case IV. From this figure, we can see the following. (i) For Case I and Case II, the lowest eigenvalues $\omega_1 = \omega_2$ do not change with the interaction, which indicates that the lowest dipole mode in an external harmonic potential, corresponding to a rigid motion of the center of mass, is independent of the nature of interatomic forces [20, 43]. In addition, for any interaction parameter β and λ, the Bogoliubov eigenvalue $\omega_1 = \omega_2 = 1$ agrees well with Lemma 2. Moreover, we observe that the multiplicity of eigenvalue ω_7 is one and the multiplicity of $\omega_1, \omega_3, \omega_5$, and ω_8 is two. (ii) For Case III and Case IV, there exist the Bogoliubov eigenvalues $\omega_j = 1, \pi$ for any β and λ. As the interaction strength changes, there is an order exchange between the fourth and fifth eigenvalue with one of them being π, and the changing point is $\lambda \approx 251.24$ for Case III and $\beta \approx 275.10$ for Case IV. The order exchange corresponds to excitation energy degeneracy, and it may also occur for other eigenvalues, e.g., between ω_7 and ω_8 in both Case III and Case IV. The physical mechanism behind is quite complicated and nontrivial, especially when it happens in higher modes. Hence we shall leave it as future work.

Example 4. Here, we consider the effect of the dipole orientation $\boldsymbol{n}$ to the Bogoliubov amplitudes $(\boldsymbol{u}, \boldsymbol{v})$ of the BdGEs with symmetric/asymmetric harmonic po-

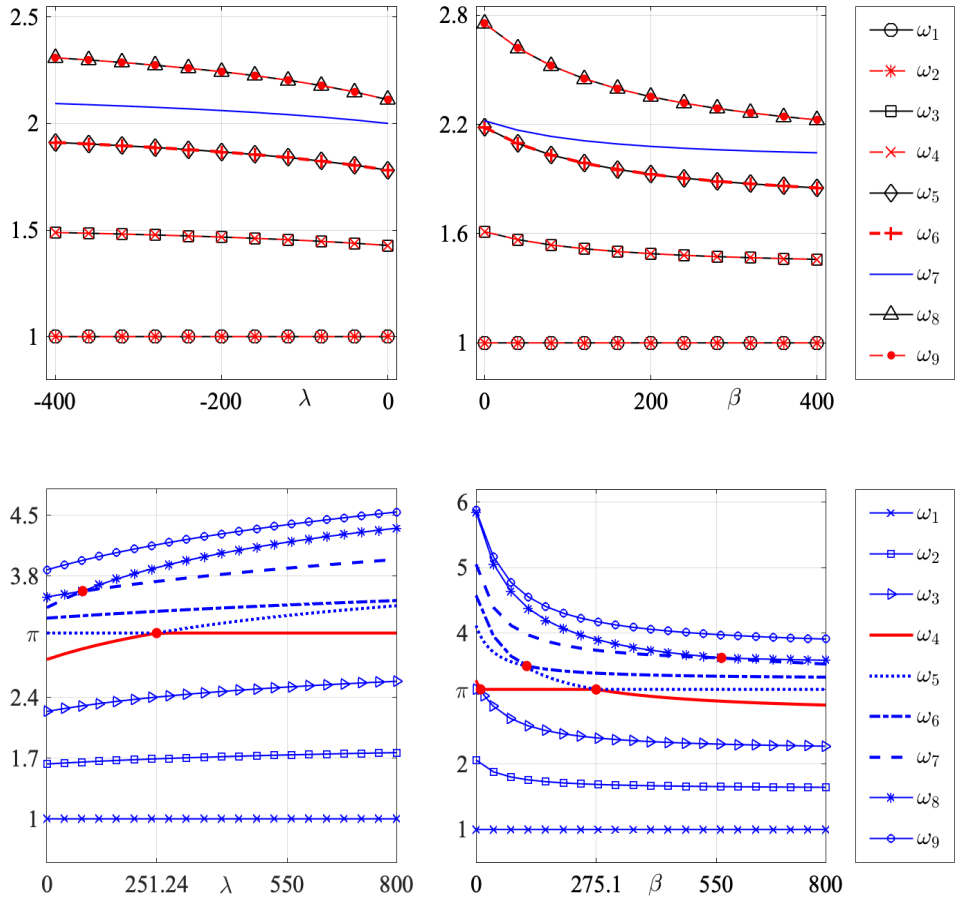

FIG. 1. *The nine smallest eigenvalues* ω_ℓ $(\ell = 1, \ldots, 9)$ *of the BdGEs for Case* I–*Case* IV *(from top left to bottom right) in Example* 3.

tentials in two dimensions. To this end, we let $\beta = 500$ and $\lambda = 400$ and study the following three cases.

Case I. $\gamma_x = \gamma_y = 1$, $\boldsymbol{n} = (1, 0, 0)^T$.
Case II. $\gamma_x = \gamma_y = 1$, $\boldsymbol{n} = (\sqrt{2}/2, \sqrt{2}/2, 0)^T$.
Case III. $\gamma_x = 1$, $\gamma_y = \pi$, $\boldsymbol{n} = (1, 0, 0)^T$.

Figure 2 displays the numerical solutions $(\boldsymbol{u}_\ell, \boldsymbol{v}_\ell)$ of the BdGEs that are associated with the first four positive eigenvalues ω_ℓ $(\ell = 1, 2, 3, 4)$ for Case I–Case III. From this figure we can see that both the dipole orientation and external potential affect the shape of the eigenvector $(\boldsymbol{u}_\ell, \boldsymbol{v}_\ell)$ essentially and significantly. The eigenvectors $(\boldsymbol{u}_\ell, \boldsymbol{v}_\ell)$ $(\ell = 1, 2, 3, 4)$ are symmetric or antisymmetric along the dipole orientation in a symmetric external potential. Meanwhile the eigenvectors will be compressed along the direction with larger trapping frequency. Indeed, the presences of DDI and anisotropic external potential bring many more rich phase diagrams for eigenmodes of BdGEs, which will be detailed in future.

Example 5. Here, we consider the 3D case. We fixed $\beta = 100$ and $\lambda = 90$ and study the following two cases.

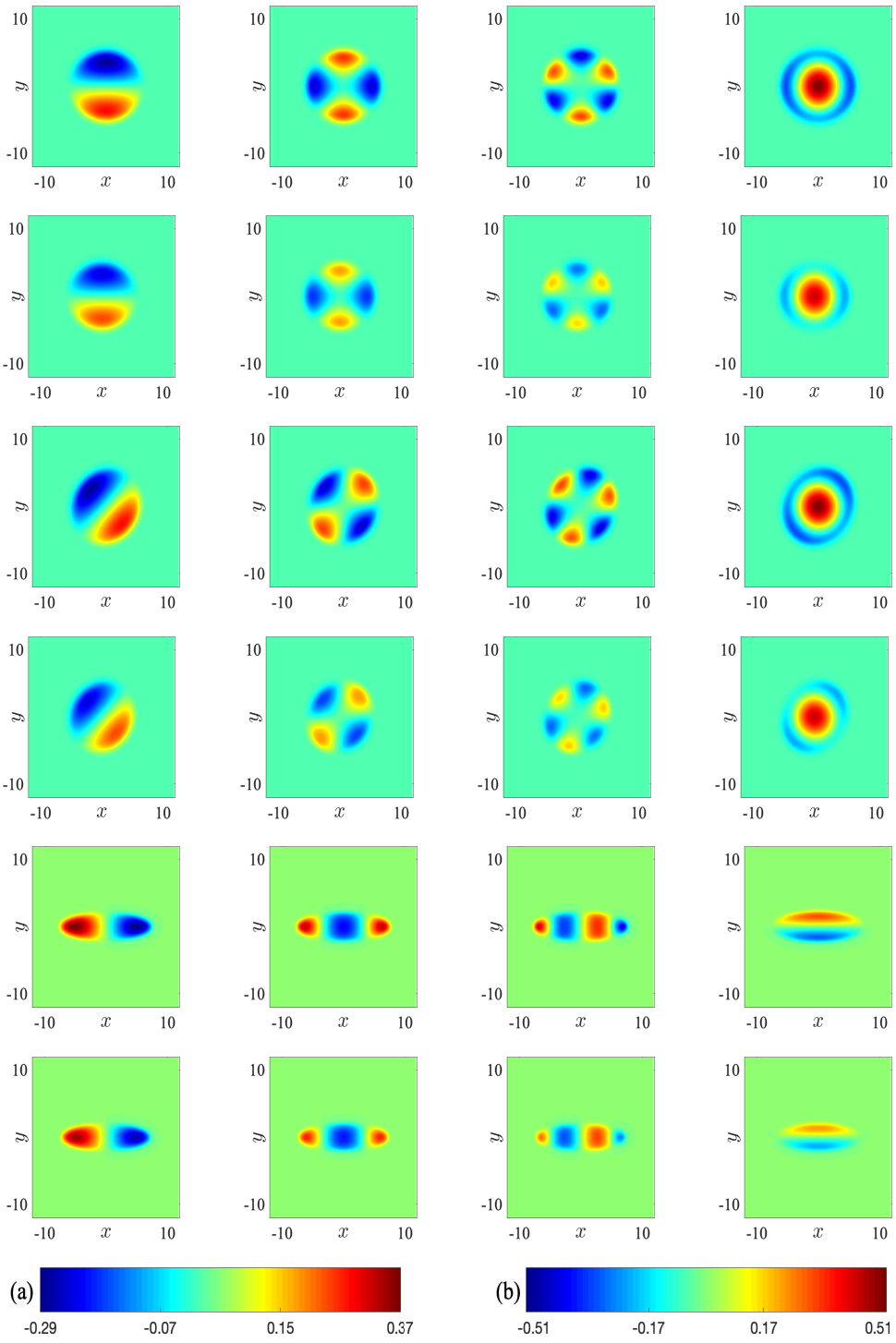

FIG. 2. *Contour plots of the Bogoliubov amplitudes* $(\boldsymbol{u}_\ell, \boldsymbol{v}_\ell)$ $(\ell = 1, \ldots, 4)$ *in Example* 4 *for Case* I *(the first two rows), Case* II *(the* 3*rd and* 4*th row), and Case* III *(the last two rows) with odd rows for* $\boldsymbol{u}_\ell$ *and even rows for* $\boldsymbol{v}_\ell$ *(from left to right* $\ell = 1, \ldots, 4$*) as well as the colorbars for Case* I*-Case* II (a) *and Case* III (b).

Case I. Symmetric potential: $\gamma_x = \gamma_y = \gamma_z = 1$. Let $\boldsymbol{n} = (1, 0, 0)^T$.

Case II. Asymmetric potential: $\gamma_x = \gamma_z = 1$, $\gamma_y = 2$. Let $\boldsymbol{n} = (0, 0, 1)^T$.

Figure 3 shows the isosurface plots of the eigenvectors $(\boldsymbol{u}_\ell, \boldsymbol{v}_\ell) = (10^{-3}, 10^{-3})$ $(\ell = 1, \ldots, 4)$ that are associated with the first four smallest positive eigenvalues ω_ℓ $(\ell = 1, \ldots, 4)$ for Case I. Figure 4 shows those associated with the first five smallest eigenvalues for Case II. Note that the multiplicity of $\omega_1 = 1$ is three and two for Case I and Case II, respectively, hence there exists three (two) independent eigenvectors for Case I (Case II). Here we only present $(\boldsymbol{u}_1, \boldsymbol{v}_1)$ simply because the other modes are quite similar. Similar to the 2D cases, we could see that both the dipole orientation and external potential affect the shape of the eigenvectors essentially and significantly. The eigenvectors $(\boldsymbol{u}_\ell, \boldsymbol{v}_\ell)$ $(\ell = 1, 2, 3, 4)$ are (anti)symmetric along the dipole orientation

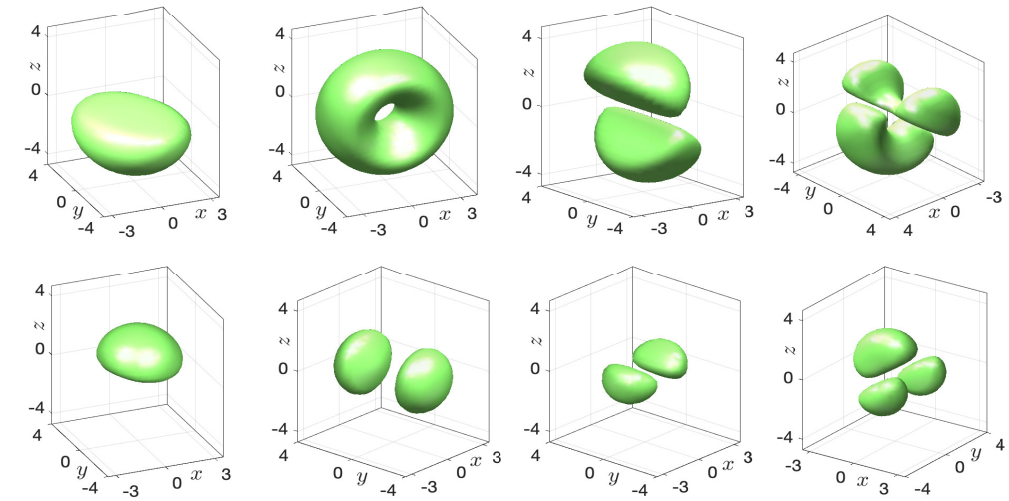

FIG. 3. *Isosurface plots of the Bogoliubov amplitude of* $\boldsymbol{u}_\ell = 10^{-3}$ *(upper) and* $\boldsymbol{v}_\ell = 10^{-3}$ *(lower) (left to right:* $\ell = 1, \ldots, 4$*) for Case* I *in Example* 5.

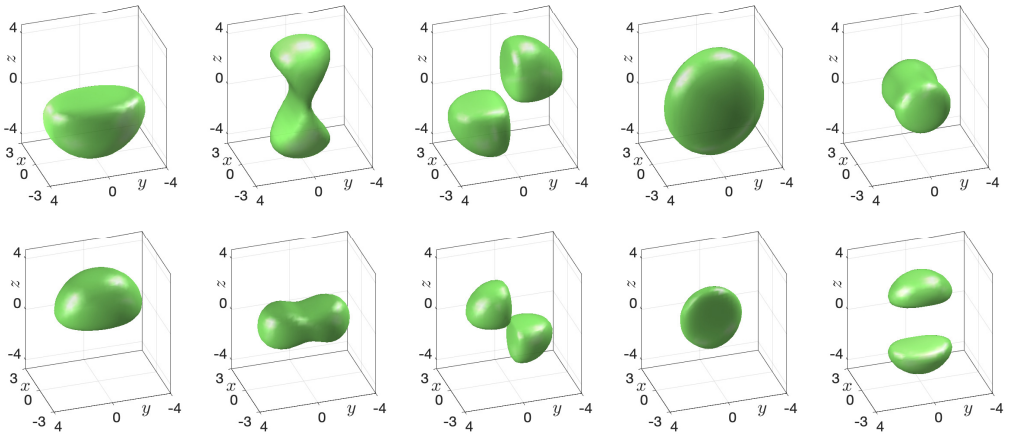

FIG. 4. *Isosurface plots of the Bogoliubov amplitude of* $\boldsymbol{u}_\ell = 10^{-3}$ *(upper) and* $\boldsymbol{v}_\ell = 10^{-3}$ *(lower) (left to right:* $\ell = 1, \ldots, 5$*) for Case* II *in Example* 5.

in a symmetric external potential, and the eigenfunctions are more compressed in the stronger trapping direction.

5. Conclusion. We proposed an efficient spectrally accurate method to compute the BdGEs (with nonlocal DDI term) characterizing the elementary excitations of dipolar BECs. Combining together the Fourier spectral method for spatial discretization, the simple Fourier spectral convolution method for evaluation of the nonlocal DDI, and the matrix-free IRAM for the discrete eigenvalue problem, the proposed method is numerically confirmed to be highly efficient (with $O(N \log N)$ operations) and of spectral accuracy. We then apply our method to investigate the effect of various parameters, including the external trapping potential, the interaction strength, and the dipole orientation to the Bogoliubov excitations in both two and three dimensions. The corresponding distributions of the excitation spectrum are illustrated, and the Bogoliubov amplitudes are also presented. In addition, we obtained analytically the first few nontrivial eigenvalues and the associated eigenvectors when the harmonic potentials are employed. Our proposed methods could be easily extended to investigating the excitation spectrums for other systems such as the rotating dipolar BEC and spinor-dipolar BEC, and we shall report them in our future work.

Acknowledgments. This work was partially done while Yong Zhang and Q. Tang were visiting the Institute for Mathematical Sciences, National University of Singapore in 2020.

REFERENCES

[1] Advanpix, Multiprecision Computing Toolbox, Version: 4.7.0 Build 13589, https://www.advanpix.com.

[2] K. Aikawa, A. Frisch, M. Mark, S. Baier, A. Rietzler, R. Grimm, and F. Ferlaino, *Bose-Einstein condensation of erbium*, Phys. Rev. Lett., 108 (2012), 210401.

[3] X. Antoine and R. Duboscq, *Robust and efficient preconditioned Krylov spectral solvers for computing the ground states of fast rotating and strongly interacting Bose-Einstein condensates*, J. Comput. Phys., 258 (2014), pp. 509–523.

[4] X. Antoine, A. Levitt, and Q. Tang, *Efficient spectral computation of the stationary states of rotating Bose-Einstein condensates by preconditioned nonlinear conjugate gradient methods*, J. Comput. Phys., 343 (2017), pp. 92–109.

[5] X. Antoine, Q. Tang, and Y. Zhang, *A preconditioned conjugated gradient method for computing ground sates of rotating dipolar Bose-Einstein condensates via kernel truncation method for dipole-dipole interaction evaluation*, Commun. Comput. Phys., 24 (2018), pp. 966–988.

[6] Z. Bai and R. C. Li, *Minimization principles for the linear response eigenvalue problem* I: *Theory*, SIAM J. Matrix Anal. Appl., 33 (2012), pp. 1075–1100.

[7] Z. Bai and R.C. Li, *Minimization principles for linear response eigenvalue problem* II: *Computation*, SIAM J. Matrix Anal. Appl., 34 (2013), pp. 392–416.

[8] D. Baillie, R. M. Wilson, and P. B. Blakie, *Collective excitations of self-bound droplets of a dipolar quantum fluid*, Phys. Rev. Lett., 119 (2017), 255302.

[9] W. Bao and Y. Cai, *Mathematical theory and numerical methods for Bose-Einstein condensation*, Kinet. Relat. Models, 6 (2013), pp. 1–135.

[10] W. Bao, Y. Cai, and H. Wang, *Efficient numerical methods for computing ground states and dynamics of dipolar Bose-Einstein condensates*, J. Comput. Phys., 229 (2010), pp. 7874–7892.

[11] W. Bao, I. Chern, and F. Y. Lim, *Efficient and spectrally accurate numerical methods for computing ground and first excited states in Bose-Einstein condensates*, J. Comput. Phys., 219 (2006), pp. 836–854.

[12] W. Bao, H. Jian, N. J. Mauser, and Y. Zhang, *Dimension reduction of the Schrödinger equation with Coulomb and anisotropic confining potentials*, SIAM J. Appl. Math., 73 (2013), pp. 2100–2123.

[13] W. Bao, S. Jiang, Q. Tang, and Y. Zhang, *Computing the ground state and dynamics of the nonlinear Schrödinger equation with nonlocal interactions via the nonuniform FFT*, J. Comput. Phys., 296 (2015), pp. 72–89.
[14] W. Bao, Q. Tang, and Y. Zhang, *Accurate and efficient numerical methods for computing ground states and dynamics of dipolar Bose-Einstein condensates via the nonuniform FFT*, Commun. Comput. Phys., 19 (2016), pp. 1141–1166.
[15] W. Bao, L. Treust, and F. Mehats, *Dimension reduction for dipolar Bose-Einstein condensates in the strong interaction regime*, Kinet. Relat. Models, 10 (2017), pp. 553–571.
[16] M. A. Baranov, *Theoretical progress in many-body physics with ultracold dipolar gases*, Phys. Rep., 464 (2008), pp. 71–111.
[17] Y. Cai, M. Rosenkranz, Z. Lei, and W. Bao, *mean field regime of trapped dipolar Bose-Einstein condensates in one and two dimensions*, Phys. Rev. A, 82 (2010), 043623.
[18] I. Danaila and F. Hecht, *A finite element method with mesh adaptivity for computing vortex states in fast-rotating Bose-Einstein condensates*, J. Comput. Phys., 229 (2010), pp. 6946–6960.
[19] I. Danaila, M. A. Khamehchi, V. Gokhroo, P. Engels, and P. G. Kevrekidis, *Vector dark-antidark solitary waves in multicomponent Bose-Einstein condensates*, Phys. Rev. A, 94 (2016), 053617.
[20] M. Edwards, P. A. Ruprecht, K. Burnett, R. J. Dodd, and C. W. Clark, *Collective excitations of atomic Bose-Einstein condensates*, Phys. Rev. Lett., 77 (1996), pp. 1671–1674.
[21] L. Exl, N. J. Mauser, and Y. Zhang, *Accurate and efficient computation of nonlocal potentials based on Gaussian-sum approximation*, J. Comput. Phys., 327 (2016), pp. 629–642.
[22] C. Eberlein, S. Giovanazzi, and D. H. G. O'Dell, *Exact solution of the Thomas–Fermi equation for a trapped Bose-Einstein condensate with dipole-dipole interactions*, Phys. Rev. A, 71 (2005), 033618.
[23] I. Ferrier-Barbut, H. Kadau, M. Schmitt, M. Wenzel, and T. Pfau, *Observation of quantum droplets in a strongly dipolar Bose gas*, Phys. Rev. Lett., 116 (2016), 215301.
[24] Y. Gao and Y. Cai, *Numerical methods for Bogoliubov–de Gennes excitations of Bose-Einstein condensates*, J. Comput. Phys., 403 (2020), 109058.
[25] L. Greengard, S. Jiang, and Y. Zhang, *The anisotropic truncated kernel method for convolution with free-space Green's functions*, SIAM J. Sci. Comput., 38 (2018), pp. A3733–A3754.
[26] K. Góral, K. Rzayewski, and T. Pfau, *Bose-Einstein condensation with magnetic dipole-dipole forces*, Phys. Rev. A, 61 (2000), 051601(R).
[27] A. Griesmaier, J. Werner, S. Hensler, J. Stuhler, and T. Pfau, *Bose-Einstein condensation of chromium*, Phys. Rev. Lett., 94 (2005), 160401.
[28] B. Hu, G. Huang, and Y. L. Ma, *Analytical solutions of the Bogoliubov-de Gennes equations for excitations of a trapped Bose-Einstein-condensed gas*, Phys. Rev. A, 69 (2004), 063608.
[29] L. Jia, A.-B. Wang, and S. Yi, *Low-lying excitations of vortex lattices in condensates with anisotropic dipole-dipole interaction*, Phys. Rev. A, 97 (2018), 043614.
[30] S. Jia, H. Xie, M. Xie, and F. Xu, *A full multigrid method for nonlinear eigenvalue problems*, Sci. China Math., 59 (2016), pp. 2037–2048.
[31] S. Jiang, L. Greengard, and W. Bao, *Fast and accurate evaluation of nonlocal Coulomb and dipole-dipole interactions via the nonuniform FFT*, SIAM J. Sci. Comput., 36 (2014), pp. B777–B794.
[32] D. S. Jin, J. R. Ensher, M. R. Matthews, C. E. Wieman, and E. A. Cornell, *Collective excitations of a Bose-Einstein condensate in a dilute gas*, Phys. Rev. Lett., 77 (1996), pp. 420–423.
[33] H. Kadau, M. Schmitt, M. Wenzel, C. Wink, T. Maier, I. Ferrier-Barbut, and T. Pfau, *Observing the Rosensweig instability of a quantum ferrofluid*, Nature, 530 (2016), pp. 194–197.
[34] P. G. Kevrekidis and D. E. Pelinovsky, *Distribution of eigenfrequencies for oscillations of the ground state in the Thomas-Fermi limit*, Phys. Rev. A, 81 (2010), 023627.
[35] T. Lahaye, C. Menotti, L. Santos, M. Lewenstein, and T. Pfau, *The physics of dipolar bosonic quantum gases*, Rep. Progr. Phys., 72 (2009), 126401.
[36] A. J. Leggett, *Bose-Einstein condensation in the alkali gases: Some fundamental concepts*, Rev. Modern Phys., 73 (2001), pp. 307–356.
[37] M. Lu, N. Q. Burdick, S. H. Youn, and B. L. Lev, *Strongly dipolar Bose-Einstein condensate of dysprosium*, Phys. Rev. Lett., 107 (2011), 190401.
[38] A. M. Martin, N. G. Marchant, D. H. J. O'Dell, and N. G. Parker, *Vortices and vortex lattices in quantum ferrofluids*, J. Phys. Condens. Matter, 29 (2017), 103004.
[39] S. A. Morgan, S. Choi, K. Burnett, and M. Edwards, *Nonlinear mixing of quasiparticles in an inhomogeneous Bose condensate*, Phys. Rev. A, 57 (1998), 3818.

[40] S. Ronen, D. C. E. Bortolotti, and J. L. Bohn, *Bogoliubov modes of a dipolar condensate in a cylindrical trap*, Phys. Rev. A, 74 (2006), 013623.
[41] C. A. Rozzi, D. Varsano, A. Marini, E. K. U. Gross, and A. Rubio, *Exact Coulomb cutoff technique for supercell calculations*, Phys. Rev. B, 73 (2006), 205119.
[42] Y. Saad, *Numerical Methods for Large Eigenvalue Problems*, Society for Industrial and Applied Mathematics, Philadelphia, 2011.
[43] S. Stringari, *Collective excitations of a trapped Bose-condensed gas*, Phys. Rev. Lett., 77 (1996), pp. 2360–2363.
[44] M. Schmitt, M. Wenzel, F. Böttcher, I. Ferrier-Barbut, and T. Pfau, *Self-bound droplets of a dilute magnetic quantum liquid*, Nature, 539 (2016), pp. 259–262.
[45] Q. Tang, H. Wang, S. Zhang, and Y. Zhang, *An efficient anisotropic method for computing the ground state and dynamics of the rotating dipolar BEC*, in preparation.
[46] The ARPACK homepage, Version: 2.1, https://www.caam.rice.edu/software/ARPACK/
[47] F. Vico, L. Greengard, and M. Ferrando, *Fast convolution with free-space Green's functions*, J. Comput. Phys., 323 (2016), pp. 191–203.
[48] H. Wang, *A projection gradient method for computing ground state of spin-2 Bose-Einstein condensates*, J. Comput. Phys., 274 (2014), pp. 473–488.
[49] R. Wilson, S. Ronen, and J. L. Bohn, *Stability and excitations of a dipolar Bose-Einstein condensate with a vortex*, Phys. Rev. A, 79 (2009), 013621.
[50] X. Wu, Z. Wen, and W. Bao, *A regularized Newton method for computing ground states of Bose-Einstein condensates*, J. Sci. Comput., 73 (2017), pp. 303–329.
[51] H. Xie and M. Xie, *A multigrid method for ground state solution of Bose-Einstein condensates*, Commun. Comput. Phys., 19 (2016), pp. 648–662.
[52] S. Yi and L. You, *Trapped condensates of atoms with dipole interactions*, Phys. Rev. A, 63 (2001), 053607.